IEEE Access
Multidisciplinary | Rapid Review | Open Access Journal

Received April 2, 2020, accepted April 9, 2020, date of publication April 22, 2020, date of current version May 6, 2020.

Digital Object Identifier 10.1109/ACCESS.2020.2988581

Effect of Symmetrical Voltage Sag on Induction Motor Considering Phase-Angle Factors Based on a New 2-D Multi-Slice Time-Stepping Finite Element Method

TIANHAO LIU[1,2], (Member, IEEE), MEIHUI JIANG[3], DONGDONG ZHANG[1], (Member, IEEE), HAISEN ZHAO[4], (Senior Member, IEEE), AND FENG SHUANG[1]

[1]School of Electrical Engineering, Guangxi University, Nanning 530004, China
[2]Department of Electrical and Electronic Engineering, University of Hong Kong, Hong Kong
[3]Nanning Freight Center, China Railway Nanning Group Company, Ltd., Nanning 530000, China
[4]State Key Laboratory of Alternate Electrical Supply System With Renewable Energy Sources, North China Electric Power University, Beijing 102206, China

Corresponding author: Dongdong Zhang (dongdongzhang@yeah.net)

This work was supported in part by the National Natural Science Foundation of China under Grant 61720106009.

ABSTRACT Voltage sag is one of the most common power quality disturbance in industry, which causes huge inrush current and inrush torque of induction motors, and has serious impacts on the safe and stable operation of induction motor. To further study the detailed transient characteristics of induction motors during sag events, an improved 2-D multi-slice field-circuit-motion coupling time-stepping finite element method (FEM) is proposed. Then, taking a 5.5 kW, a 55 kW and a 135 kW induction motors as examples, the influence of phase-angle jumps and initial point-on-wave on the stator current peak, torque peak, speed loss and critical clearing time of the induction motor are discussed by using the proposed model. The simulation results show that stator current peak and torque peak increase obviously, while speed and critical clearing time decrease apparently, when considering the phase angle jump. And different initial points have little influence on these operation indicators. Finally, the proposed method is verified by comparing the measured and calculation data of the 5.5 kW three-phase squirrel-cage motor, respectively. The results show that the proposed method can reach higher precision with considering nonlinear characteristics.

INDEX TERMS INDEX TERMS voltage sag, induction motors, phase-angle factor, finite element method, power quality.

I. INTRODUCTION

With the development of technologies and production requirements, power users demand higher power quality [1]–[3]. Voltage sag is one of the main power-quality (PQ) problems for typical industrial customers; and nearly 80% PQ problems are caused by voltage sag [4]–[7]. As a widely applied equipment in industrial production, induction motors are influenced by voltage sags in two main aspects: i) inrush current and inrush torque caused by voltage sags may intrigue the action of current protective devices, which leads to the interruption of the operation, and damage the rotor shaft; ii) long ride through time for induction motors with heavy load may lead to stalling and burnout of motor. Therefore, it is necessary to deeply study the effect of voltage sag on the performance of induction motors in order to provide theories for the motor's steady and safe operation.

Voltage sag is defined as a short-duration reduction in RMS (root mean square) voltage at a point of the power system which can be caused by a short circuit, overload or starting of electric motors [4], [8]. In a voltage sag event, the voltage magnitude drops from 90% to 10% of the nominal value and lasts from half cycle to one minute [9]–[12]. The characteristics of voltage sag are magnitude, duration, phase-angle jump and initial phase angle. According to statistics, most voltage sags have a duration from four to ten cycles, and phase-angle jump from $-60°$ to $10°$ [13]–[16]. The main research methods about the motor operation under voltage sag

The associate editor coordinating the review of this manuscript and approving it for publication was Pinjia Zhang.

include analytical method, numerical algorithm, finite element method (FEM) and experiment [17]–[20]. For example, in [21] an analytical method is presented to determine the maximum symmetrical voltage sag ride through time, namely critical clearance time, for induction motors. An analytical method is used for calculating the inrush stator current during sag process in [22]. Analytical study of the dynamic behavior of the doubly fed induction generator subject to the voltage sag is discussed in [23]. However, in the analytical algorithm, the strong hypothesis, i.e. constant rotor speed, cause the observable error in the sag process analysis. Therefore, numerical algorithm is used for precisely calculating with considering rotor speed loss [24]–[31]. In [24], a numerical algorithm is introduced for the approximate calculation of the current and torque peaks, and the mechanical speed loss for an extensive range of voltage sags and finds that the values of peak current and torque increase linearly with the decrease of voltage sag magnitude. In [25], the effects of different voltage sags are studied on the behaviors of induction motors by using a MATLAB/Simulink software. The consequences of unsymmetrical voltage sags on the torque and current peaks, and speed loss characteristics of three-phase squirrel-cage induction motor is analyzed based on the numerical algorithm in [26]–[28]. The behavior of different types of motors, such as single- and double-cage induction models, under the symmetrical voltage sag is also considered in [29]. As for symmetrical voltage sag, [26], [29] find that the average values of peak current and peak torque caused by symmetrical voltage sags in different situations are more serious than that caused by unsymmetrical voltage sags. In [30], [31], the interaction between induction motors and voltage sags are studied based on PSCAD/EMTDC package. However, as for the numerical algorithm, the skin effect, nonlinear behaviors of magnetic materials, and the end-ring effect cannot be considered. Experimental study and some calculations of a standard three-phase squirrel-cage motor of 5.5 kW induction motor behavior is proposed, and the study found that the motor re-acceleration duration and magnitudes are determined by the interaction between motor load, system hot-load pickup, and voltage sag magnitude in [32]. Although the experiment test has precise results, in many situations, it's very difficult to carry out the experiment the induction motor rated 20 kW and higher [33]. In addition, it is also hard to measure magnetic flux density distribution and current density distribution. Compared to the above methods, FEM is an effective simulation method to analyze the operation characteristics of induction motors [34], [35].

In previous studies, the main independent variables (indices) of voltage sag analysis include sag type, magnitude, duration and load condition and the main dependent variables (indices) of voltage sag analysis includes current peak, torque peak, mechanical speed loss and critical clearance time [24]–[29]. However, in most situations, the voltage sag not only causes drop of voltage magnitude, but also results in the phase angle jump. Therefore, considering only one sag index, i.e. sag magnitude, will cause noticeable error. The initial point-on-wave has different influences on symmetrical and unsymmetrical voltage sags. As for the effect of phase-angle factors: phase-angle jump and initial point-on-wave on induction motor, further studies are still needed.

In order to study the effect of phase-angle factors on the performance of induction motor during the process of voltage sag, a new 2-D multi-slice time-stepping FEM is applied to model the motor's performances. The main conclusions are as follow:

1) A new 2-D multi-slice time-stepping FEM is proposed for voltage sag process. Different from 2-D time stepping FEM and 3-D FEM, 2-D multi-slice can consider the asymmetric rotor structure of the motor with less computation cost. However, the traditional 2-D multi-slice FEM cannot accurately calculate the transient performance of the induction motor. In this paper, the traditional 2-D multi-slice FEM are extended to combine the field, current constraint, circuit and mechanical motion equations.

2) The influence of the combination of two sag indices: sag magnitude and phase angle jump on induction motor's current peak, torque peak, speed loss and critical clearance time during the sag process is studied.

3) The different influence of initial phase angle during symmetrical and unsymmetrical voltage sags process on induction motor's current peak, torque peak, speed loss and critical clearance time is analysed and summarized.

The rest of this paper is organized as follows. In section II, the cause of phase-angle jumps and the relationship between sag magnitude and phase-angle jump are studied. In section III, a new 2-D multi-slice time-stepping FEM for voltage sag process is introduced. In section IV, the effect of two sag indices: sag magnitude and phase-angle jump on the motor performance during voltage sag process is analyzed. In section V, the difference of the initial phase angle's influence on the motor performance between symmetrical voltage sag process and unsymmetrical voltage sag process are studied. In section VI, the accuracy and computation efficiency of the proposed method are verified by using a real test of the standard 5.5 kW three-phase squirrel-cage motor. The conclusion is drawn in Section VII

II. ANALYSIS OF VOLTAGE SAG CHARACTERISTICS

The typical voltage sag waveform is shown in Fig. 1. It can be seen that a complete voltage sag process contains two jump times. One is beginning time and the other is the moment of returning to normal voltage after a sag duration. Voltage phase of beginning time is called initial point-on-wave. The voltage phase of the moment of returning to normal voltage is called recovery point-on-wave. In this paper initial and recovery point of three phase are especially referred to phase A. The main voltage sag characteristics mainly include sag magnitude, sag duration, phase-angle jump and initial point-on-wave. Sag magnitude is defined as the ratio of RMS value of the voltage during sag process to rms value of the rated voltage. Sag duration is defined as the time from the

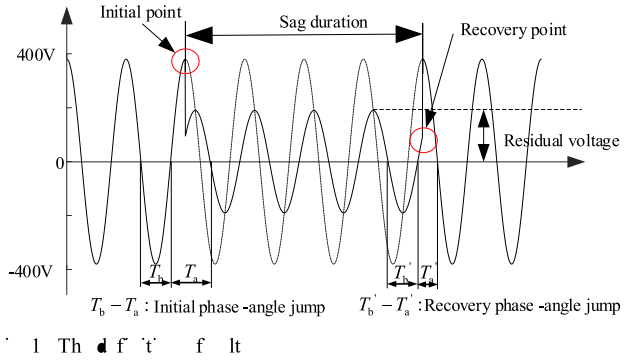

FIGURE 1. The definition of voltage sag.

occurrence to the end. In addition, most of voltage sags are accompanied by the phase jumps [36].

The main reasons of phase-angle jump are: i) Difference of impedance angle between the system and the distribution line; ii) Unbalanced voltage sags distribute to the low voltage system. Since symmetrical voltage sag is mainly considered, this paper only takes account into the factor of mismatch of the system and the line impedance.

$Z_1 = R_1 + jX_1$ is system impedance and $Z_2 = R_2 + jX_2$ is line impedance, as show in Fig. 2. Load current is ignored and we assume that $\dot{U}_S = 1\angle 0°$. The voltage of PCC (point of common coupling):

$$\dot{U}_{sag} = \frac{Z_2}{Z_1 + Z_2} \tag{1}$$

And phase-angle jump can be obtained by (2):

$$\alpha = \arg(\dot{U}_{sag}) - \arg(\dot{U}_s) = tg^{-1}(\frac{Z_2}{R_2}) - tg^{-1}(\frac{Z_1 + Z_2}{R_1 + R_2}) \tag{2}$$

Let $\xi = R_2/R_1, k_1 = X_1/R_1, k_2 = X_2/R_2$. The (3) can be obtained by combining (1) and (2):

$$\begin{cases} \left(1 + k_2^2\right)\left(1 - U_{sag}^2\right)\xi^2 - U_{sag}^2\left(2 + 2k_1k_2\right)\xi \\ \quad - \left(1 + k_1^2\right)U_{sag}^2 = 0 \\ \arg\left(\dot{U}_{sag}\right) = tg^{-1}k_2 - tg^{-1}\left(k_2 - \dfrac{k_2 - k_1}{1 + \zeta}\right) \end{cases} \tag{3}$$

From (3), it can be seen that voltage phase-angle jump is determined by k_1, k_2 and U_{sag}. Therefore, the phase-angle jump is related to the sag magnitude and impedance between line and system. In most voltage sags, the phase-angle jumps

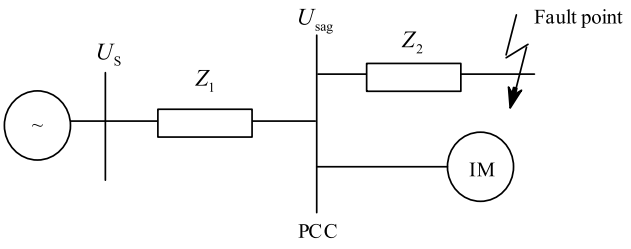

FIGURE 2. The simple equivalent circuit of power system with voltage sag.

TABLE 1. Sag magnitude and corresponding phase-angle jump angle (unit: degree).

U_{sag}	0.9	0.8	0.7	0.6	0.5	0.4	0.3	0.2	0.1
$\arg(U_{sag})$	-8.2	-15	-21	-27	-32	-38	-43	-48	-53

are between -60° ∼10°. In this paper, the distribution network with cables are taken as an example, the relationship between the sag magnitude and phase-angle jump is shown in Table 1. In distribution network with cables, $k_1 = 10$ and $k_2 = 0.5$, then (3) can be written as

$$\begin{cases} 1.25(1 - U_{sag}^2)\xi^2 - 12\xi U_{sag}^2 - 101U_{sag}^2 = 0 \\ \arg\left(\dot{U}_{sag}\right) = tg^{-1}0.5 - tg^{-1}\left(0.5 + \dfrac{9.5}{1 + \xi}\right) \end{cases} \tag{4}$$

The different phase-angle jumps which are caused by different sag magnitudes are shown in Table 1. From Table 1, different sag magnitudes are corresponding to different phase-angle jumps. In addition, initial point-on-wave is another important factor. As it is generally believed that the moment of failure is random, the angle of the voltage at initial point-on-wave is uniformly distributed between 0° and 360°.

III. MATHEMATICAL MODEL OF INDUCTION MOTOR

Time-stepping FEM is suitable for detailed analysing of the transient performances of induction motors during the voltage sag process, which includes four parts: field equations, current constraint equations, circuit equation and motion equation.

A. FIELD EQUATIONS

The electromagnetic field equation of induction motors in 2-D Cartesian coordinates can be formulated as [37]:

$$\frac{\partial}{\partial x}(\frac{1}{\mu}\frac{\partial A}{\partial x}) + \frac{\partial}{\partial y}(\frac{1}{\mu}\frac{\partial A}{\partial y}) = -J_s + \sigma\left(\frac{\partial A}{\partial t} + \nabla\Phi\right) \tag{5}$$

where A, μ, σ, J_s and Φ are the nodal magnetic vector potential, magnetic permeability, conductivity of rotor bar, current density and the electric scalar potential, respectively.

B. CURRENT CONSTRAINT EQUATION

The rotor bar currents and the stator winding currents constraint equations of the cage induction motor can be expressed as:

$$U_\Phi = l_{motor}\frac{\partial\Phi}{\partial z} = I_rR_r + \frac{l_{motor}}{S_r}\int_{S_r}\frac{\partial A}{\partial t}dS \tag{6}$$

$$U_\Phi = l_{motor}\frac{\partial\Phi}{\partial z} = R_sI_s + \frac{N_sl_{motor}}{S_c}\int_{S_c}\frac{\partial A}{\partial t}dS \tag{7}$$

where R_r, I_r, l_{motor}, S_r is the resistance of rotor bar, the rotor current, the axial length of the motor core, and the rotor bars' section area, respectively. R_s is the resistance of stator in per phase and I_s is the current of the stator winding in per phase.

C. CIRCUIT EQUATION

The circuit equation of each phase of the stator windings can be expressed as

$$U_s = (R_{Li} + R_s)\, I_s + (L_{Li} + L_{TL})\, \frac{dI_s}{dt} + \frac{d\psi}{dt} \tag{8}$$

where U_S is the terminal phase voltage, R_s is the per phase winding resistance, R_{Li} is the resistance of transmission line, I_s is the current of the stator winding per phase, L_{TL} is the leakage inductance of end turn, L_{Li} is the inductance of transmission line, and Ψ is the flux linkage of the per phase stator winding.

The total flux linkage is expressed as:

$$\Psi = K_d N_a \frac{l_{motor}}{3aS_W} \sum_{i_1=1}^{2p} \sum_{i_2=1}^{q} \sum_{i_3=1}^{N_{Snode}} \sum_{i_4=1}^{m} S_{Wi_3} A_{i_3(i_4)} \tag{9}$$

where S_{Wi3} is the i_3^{th} element area, S_W is the stator winding area, $K_d = 1$ means the positive current direction; and $K_d = -1$ means negative current direction. N_a is the number of parallel branches, N_{Snode} is the nodes number of each slot, p is the pole-pairs number, q is the slots per pole per phase, and m is the nodes number of element.

D. MOTION EQUATION

The mechanical motion equation of an induction motor is

$$\begin{cases} J_m \dfrac{d\omega}{dt} = T_e - C_f\omega - T_l \\ \omega = \dfrac{d\theta}{dt} \end{cases} \tag{10}$$

where J_m is rotational inertia, Ω is rotor mechanical angular velocity, $d\omega/dt$ is angular acceleration rate, T_e is the electromagnetic torque, T_l is the load torque, θ is the angle of rotor position, and C_f is the friction constant.

E. 2-D MULTI-SLICE FIELD-CIRCUIT-MOTION COUPLING EQUATION

The field-circuit-motion coupling matrix equation can be obtained by combining field equations, current constraint equations, circuit equation and motion equation.

The current constraint matrix equation can be obtained from (6) and (7).

$$0 = \mathbf{C}^* \frac{\partial \mathbf{A}}{\partial t} + \mathbf{R}^* \mathbf{I} - \mathbf{U}_\Phi \tag{11}$$

The stator circuit matrix equation can be obtained from (8) and (9).

$$\mathbf{U_s} = \mathbf{D_s}^* \frac{\partial \mathbf{A}}{\partial \mathbf{t}} + \mathbf{R_s}^* \mathbf{I_s} + \mathbf{L_s}^* \frac{\partial \mathbf{I_s}}{\partial \mathbf{t}} \tag{12}$$

Similarly, the current matrix equation in the rotor bars can be formulated as

$$0 = \mathbf{D_r}^* \frac{\partial \mathbf{A}}{\partial \mathbf{t}} + \mathbf{R_r}^* \mathbf{I_r} + \mathbf{L_r}^* \frac{\partial \mathbf{I_r}}{\partial \mathbf{t}} \tag{13}$$

Therefore, (12) and (13) can be rewritten as

$$\mathbf{U} = \mathbf{D}^* \frac{\partial \mathbf{A}}{\partial \mathbf{t}} + \mathbf{R}^* \mathbf{I} + \mathbf{L}^* \frac{\partial \mathbf{I}}{\partial \mathbf{t}} \tag{14}$$

In the mechanical motion equation, the electromagnetic torque can be rewritten as the function of **A** as

$$\mathbf{T_e} = \mathbf{A^T H A} \tag{15}$$

where **H** is the electromagnetic torque coefficient matrix in magnetic vector potential form. From (11) -(15), the field-circuit-motion coupling matrix can be derived as:

$$\begin{bmatrix} \mathbf{K_A} & \mathbf{K_{U\Phi}} & \mathbf{K_I} & \mathbf{0} & \mathbf{0} \\ \mathbf{0} & \mathbf{-1} & \mathbf{R} & \mathbf{0} & \mathbf{0} \\ \mathbf{0} & \mathbf{0} & \mathbf{R} & \mathbf{0} & \mathbf{0} \\ \mathbf{A^T H} & \mathbf{0} & \mathbf{0} & \mathbf{0} & \mathbf{0} \\ \mathbf{0} & \mathbf{0} & \mathbf{0} & \mathbf{1} & \mathbf{0} \end{bmatrix} \begin{bmatrix} \mathbf{A} \\ \mathbf{U_\Phi} \\ \mathbf{I} \\ \boldsymbol{\omega} \\ \theta \end{bmatrix} + \begin{bmatrix} \mathbf{D_A} & \mathbf{0} & \mathbf{0} & \mathbf{0} & \mathbf{0} \\ \mathbf{C} & \mathbf{0} & \mathbf{0} & \mathbf{0} & \mathbf{0} \\ \mathbf{D} & \mathbf{0} & \mathbf{L} & \mathbf{0} & \mathbf{0} \\ \mathbf{0} & \mathbf{0} & \mathbf{0} & \mathbf{-J_m} & \mathbf{0} \\ \mathbf{0} & \mathbf{0} & \mathbf{0} & \mathbf{0} & \mathbf{-1} \end{bmatrix} \frac{\partial}{\partial t} \begin{bmatrix} \mathbf{A} \\ \mathbf{U_\Phi} \\ \mathbf{I} \\ \boldsymbol{\omega} \\ \theta \end{bmatrix} = \begin{bmatrix} \mathbf{0} \\ \mathbf{0} \\ \mathbf{U} \\ \mathbf{T_l} \\ \mathbf{0} \end{bmatrix} \tag{16}$$

where $\mathbf{D_A}$, $\mathbf{C}$, $\mathbf{D}$ are the nodal vector magnetic potential's derivative terms matrix in the field equation, that in the current constraint equation and that in the stator and rotor winding equation, respectively. $\mathbf{K_A}$, $\mathbf{K_{U\Phi}}$, $\mathbf{K_I}$ is the stiffness matrix of field equation, that of the current constraint equation and that of the stator and rotor winding equation.

In order to consider axial asymmetries of the 5.5 kW and 55 kW induction motor with the skewed rotor bar. The induction motor can be divided into k layers along the axial direction. In each layer, induction motor can be treated as the straight rotor bar. Therefore, (17) can be used in each layer to calculate the electromagnetic properties. The equation of the 2-D multi-slice FCM coupling time stepping FEM can be formulated (17), as shown at the bottom of the next page.

IV. EFFECTS OF PHASE-ANGLE JUMP

The indices chosen to study the effects of phase-angle jump and initial point-on-wave are the torque peak, current peak, speed loss and critical clearance time. These values are calculated in p. u. (per unit). They are referred to the nominal or rated torque, current and speed, which are expressed as (18), (19) and (20), respectively.

$$\Gamma_{\text{peak}} = \frac{\Gamma_{\text{r,peak}}}{\Gamma_{\text{N}}} = \frac{\max\{|\Gamma_{\text{r}}(t)|\}}{\Gamma_{\text{N}}} \tag{18}$$

$$i_{\text{peak}} = \frac{i_{\text{r,peak}}}{\sqrt{2}I_{\text{N}}} = \frac{\max\left\{\left|i_{\text{a,r}}(t)\right|, \left|i_{\text{b,r}}(t)\right|, \left|i_{\text{c,r}}(t)\right|\right\}}{\sqrt{2}I_{\text{N}}} \tag{19}$$

$$\omega_{\text{min}} = \frac{\omega_{\text{r,min}}}{\omega_{\text{N}}} = \frac{\min\{\omega_{\text{r}}(t)\}}{\omega_{\text{N}}} \tag{20}$$

where, subscript N means nominal values and subscript r represents real value

A. EFFECTS OF PHASE-ANGLE JUMP ON CURRENT PEAK

In the previous studies [24]–[29], researchers mainly focused on sag magnitude and sag duration. However, different sag

magnitudes may result in different phase-angle jumps, which has significant influence on peak values of stator current, torque and rotor speed loss. In the paper, load conditions are selected no-load, 50% full load, and full load. According to international standard IEC 61000-4-11: 2004, starting point of voltage sag is preferentially selected 0° and sag magnitude range from 90% to 10% and most of sag durations are between one and ten cycles. In this section, sag duration is selected as 5 cycles and two situations which are with and without considering phase-angle jump are compared. The beginning time of voltage sag is set to t_0. When voltage sag happens, $u_A = U_m \sin(\omega t_0)$ change to $u_A = U_{m1}\sin(\omega t_0+\theta_1)$. After 0.1s, $u_A = U_{m1}\sin(\omega(t_0+0.1)+\theta_1)$ restore to $u_A = U_m\sin(\omega(t_0+0.1))$. When phase-angle jump is not considered, θ_1 is set to 0°. As for phase B and C, the situation is similar. The relationship between sag magnitude and phase angle jump can be obtained from Table 1. The calculated results of phase-angle jump effect on the current peak in different voltage sag magnitude is shown in Fig. 3. From Fig. 3., it can be concluded that.

1) From [25] and [32], it can be concluded that current peak almost depends linearly on sag magnitude. However, as shown in Fig. 3, this case only happens when corresponding phase angle jump are not considered. In addition, the linearity of the curve decreases with load rate increasing. From Fig. 3., it can be seen that when considering phase-angle jump, peak current curve of the motor can be considered as a similar parabola line. Therefore, the maximum peak current is not corresponding to the minimum sag magnitude. Taking the 55-kW induction motor with 50% of full load as an example, the maximum peak current value appears at the sag process with 40% sag magnitude.

2) The peak current value with considering phase-angle jump is obviously higher than the value without considering phase-angle jump. It can be concluded that ignoring the phase-angle jump may cause evaluation errors of the motor performance under voltage sags process. Taking the 55kw motor under 50% sag magnitude as an example, at full load condition, peak current with considering phase-angle jump is 70% higher than that without considering phase-angle jump; At 50% load condition, peak current with considering phase-angle jump is 50% higher than that without considering phase-angle jump; At no load condition, peak current with considering phase-angle jump is 83% higher than that without considering phase-angle jump. It is obvious that with considering phase angle jump, the peak current value is significantly higher than that without considering phase angle jump. According to American distribution network power quality (DPQ) survey, nearly 80%∼90% voltage sags are accompanied by the phase-angle jumps [36]. So not considering phase-angle jump may lead to inaccurate results, especially in the range from 30% magnitude to 70% magnitude.

B. EFFECTS OF PHASE-ANGLE JUMP ON TORQUE PEAK AND SPEED

From previous studies, the influence of corresponding phase-angle jump during voltage sag process are not taken into consideration. Fig. 4 and Fig. 5 show the torque and speed loss, respectively, produced by symmetrical voltage sag in three types motors (5.5 kW, 55 kW and 135 kW) with considering phase-angle jump during sag process from 10% to 90% magnitude.

1) From the Fig. 4, the peak torque value with phase-angle jump is obviously higher than that without phase-angle jump. Taking 55 kW motor with no load as an example, peak torque caused by voltage sag without phase-angle jump is less than 4 times rated torque. However, when considering phase-angle jump, if sag magnitude is less than 40%, peak torque is greater than 4 times rated torque. So, voltage sag without considering phase-angle may lead to a relatively lower result, which will influence the set of torque protection.

2) As shown in Fig. 5, when the motor with full load, the influence of phase- angle jump on the minimum speed

$$
\begin{bmatrix}
\mathbf{K_{A(1,\theta)}} & \mathbf{0} & \mathbf{0} & \mathbf{0} & \mathbf{K_{U_\Phi(1,\theta)}} & \mathbf{K_{I(1,\theta)}} & \mathbf{0} & \mathbf{0} \\
\mathbf{0} & \mathbf{K_{A(2,\theta)}} & \mathbf{0} & \mathbf{0} & \mathbf{K_{U_\Phi(2,\theta)}} & \mathbf{K_{I(2,\theta)}} & \mathbf{0} & \mathbf{0} \\
\mathbf{0} & \mathbf{0} & \dots & \mathbf{0} & \dots & \dots & \mathbf{0} & \mathbf{0} \\
\mathbf{0} & \mathbf{0} & \mathbf{0} & \mathbf{K_{A(k,\theta)}} & \mathbf{K_{U_\Phi(k,\theta)}} & \mathbf{K_{I(k,\theta)}} & \mathbf{0} & \mathbf{0} \\
\mathbf{0} & \mathbf{0} & \mathbf{0} & \mathbf{0} & \mathbf{-1} & \mathbf{0} & \mathbf{0} & \mathbf{R} \\
\mathbf{0} & \mathbf{0} & \mathbf{0} & \mathbf{0} & \mathbf{0} & \mathbf{R} & \mathbf{0} & \mathbf{0} \\
\mathbf{A_{(1)}^T H} & \mathbf{A_{(2)}^T H} & \dots & \mathbf{A_{(k)}^T H} & \mathbf{0} & \mathbf{0} & \mathbf{0} & \mathbf{0} \\
\mathbf{0} & \mathbf{0} & \mathbf{0} & \mathbf{0} & \mathbf{0} & \mathbf{0} & \mathbf{1} & \mathbf{0}
\end{bmatrix}
\begin{bmatrix}
\mathbf{A_{(1)}} \\ \mathbf{A_{(2)}} \\ \dots \\ \mathbf{A_{(k)}} \\ \mathbf{U_\Phi} \\ \mathbf{I} \\ \boldsymbol{\omega} \\ \theta
\end{bmatrix}
+
\begin{bmatrix}
\mathbf{D_{A(1,\theta)}} & \mathbf{0} & \mathbf{0} & \mathbf{0} & \mathbf{0} & \mathbf{0} & \mathbf{0} & \mathbf{0} \\
\mathbf{0} & \mathbf{D_{A(2,\theta)}} & \mathbf{0} & \mathbf{0} & \mathbf{0} & \mathbf{0} & \mathbf{0} & \mathbf{0} \\
\mathbf{0} & \mathbf{0} & \dots & \mathbf{0} & \mathbf{0} & \mathbf{0} & \mathbf{0} & \mathbf{0} \\
\mathbf{0} & \mathbf{0} & \mathbf{0} & \mathbf{D_{A(k,\theta)}} & \mathbf{0} & \mathbf{0} & \mathbf{0} & \mathbf{0} \\
\mathbf{C_{(1,\theta)}} & \mathbf{C_{(2,\theta)}} & \dots & \mathbf{C_{(k,\theta)}} & \mathbf{0} & \mathbf{0} & \mathbf{0} & \mathbf{0} \\
\mathbf{D_{(1,\theta)}} & \mathbf{D_{(2,\theta)}} & \dots & \mathbf{D_{(k,\theta)}} & \mathbf{0} & \mathbf{L} & \mathbf{0} & \mathbf{0} \\
\mathbf{0} & \mathbf{0} & \mathbf{L} & \mathbf{0} & \mathbf{0} & \mathbf{0} & \mathbf{-J_m} & \mathbf{0} \\
\mathbf{0} & \mathbf{0} & \mathbf{0} & \mathbf{0} & \mathbf{0} & \mathbf{0} & \mathbf{0} & \mathbf{-1}
\end{bmatrix}
\frac{\partial}{\partial t}
\begin{bmatrix}
\mathbf{A_{(1)}} \\ \mathbf{A_{(2)}} \\ \dots \\ \mathbf{A_{(k)}} \\ \mathbf{U_\Phi} \\ \mathbf{I} \\ \boldsymbol{\omega} \\ \theta
\end{bmatrix}
=
\begin{bmatrix}
\mathbf{0} \\ \mathbf{0} \\ \dots \\ \mathbf{0} \\ \mathbf{0} \\ \mathbf{U} \\ \mathbf{T_l} \\ \mathbf{0}
\end{bmatrix}
\tag{17}
$$

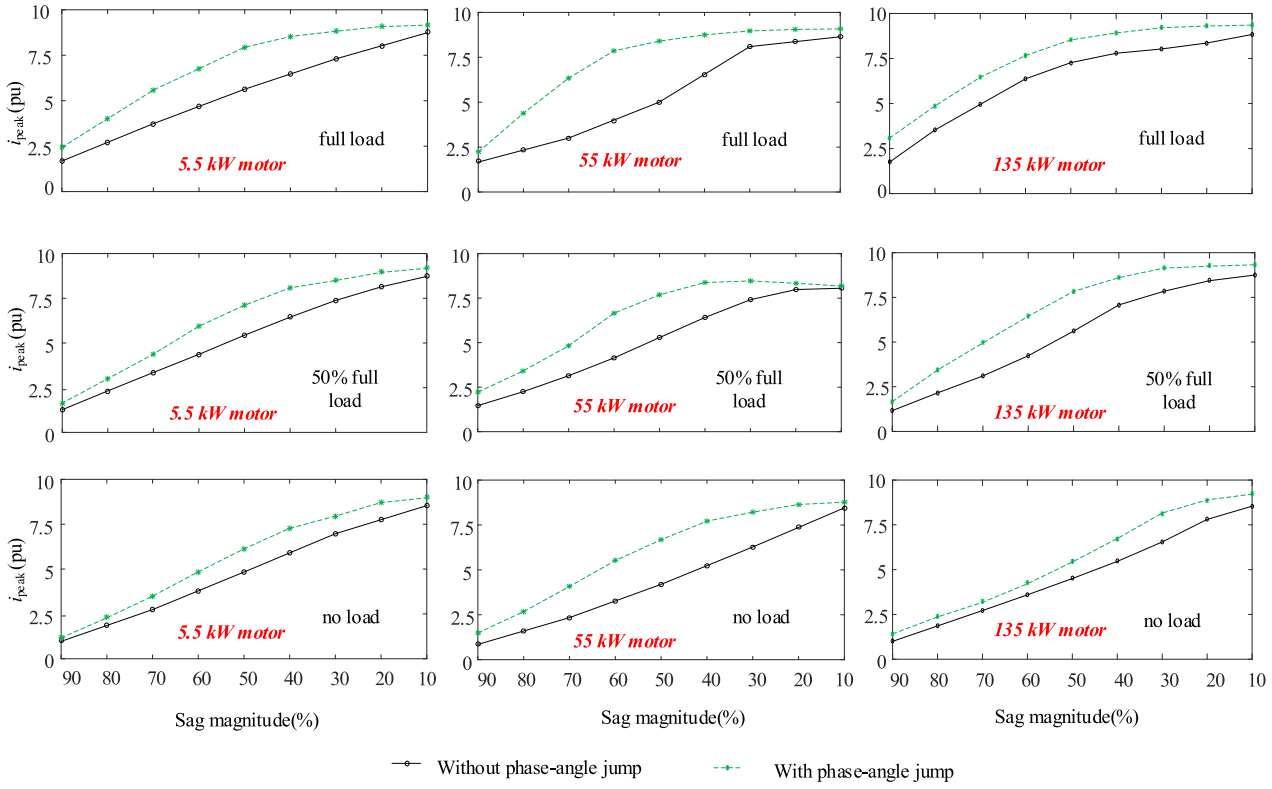

FIGURE 3. Influence of phase-angle jump on the current peak in different voltage sag magnitude.

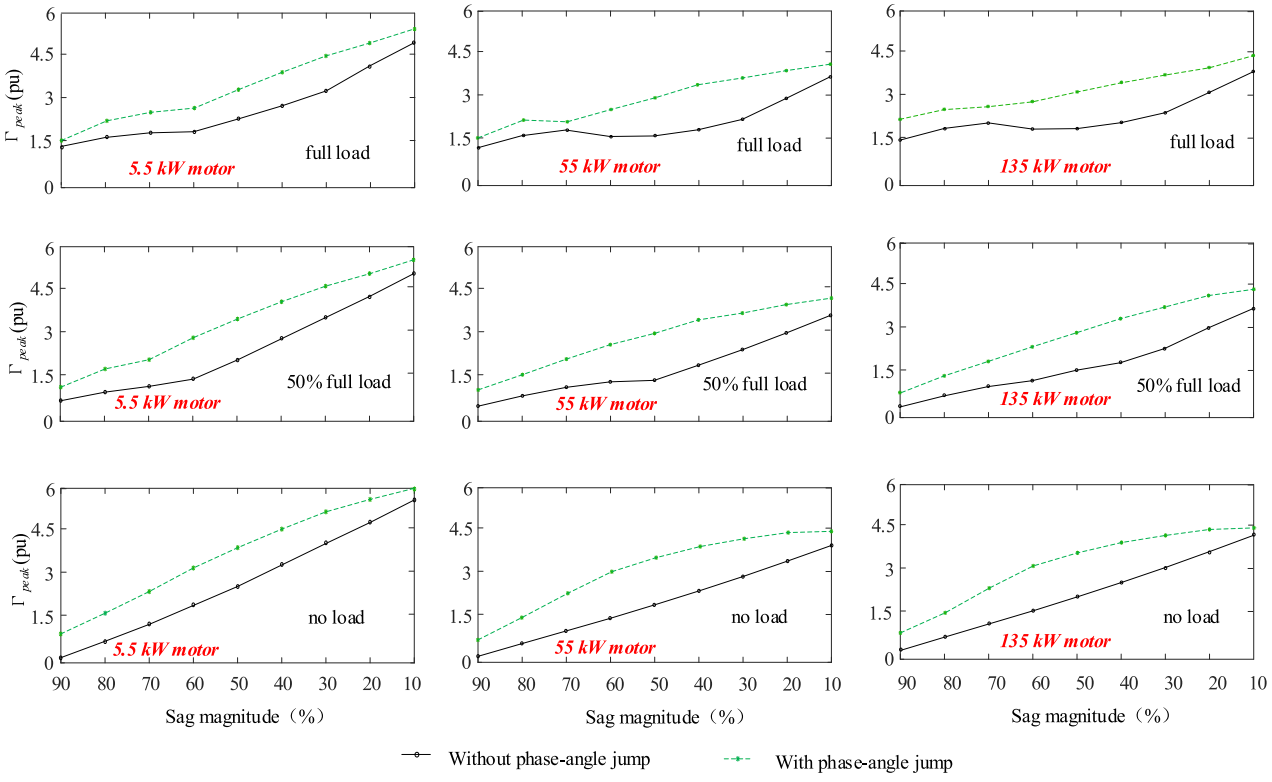

FIGURE 4. Influence of phase-angle jump on the torque peak in different voltage sag magnitude.

during the voltage sag is significant. Taking the 55-kW motor as an example, the minimum speed during the voltage sag with phase angle jump is obviously smaller than the value during the voltage sag without phase angle jump, especially in the range of sag magnitude between 30% and 70%.

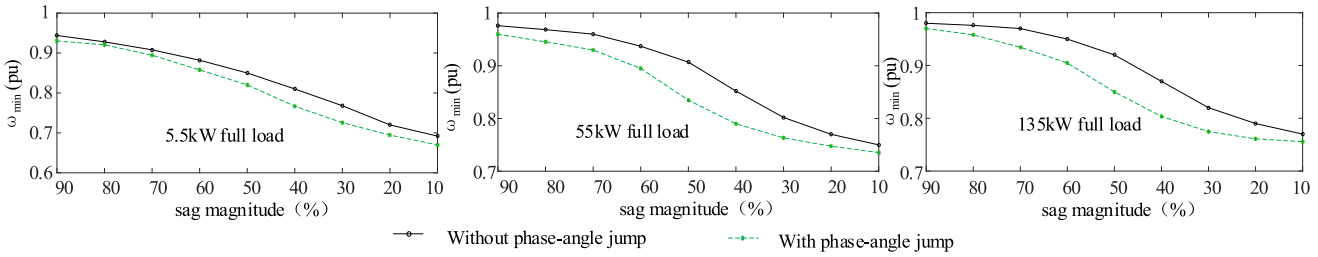

FIGURE 5. Influence of phase-angle jump on the speed loss in different voltage sag magnitude.

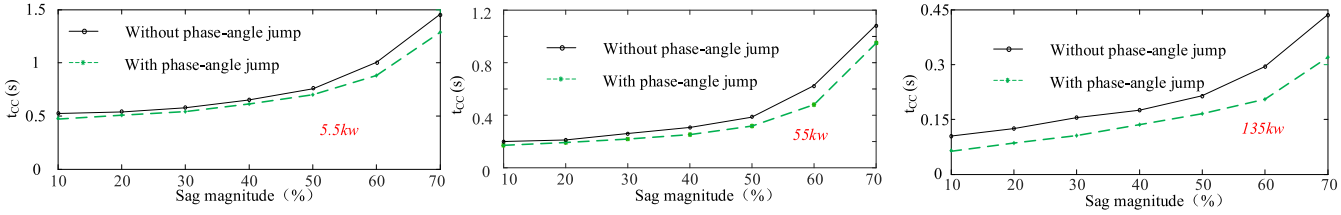

FIGURE 6. Comparison of different critical clearance time of 5.5kW, 55 kW and 135 kW motor.

C. EFFECTS OF PHASE-ANGLE JUMP ON CRITICAL CLEARANCE TIME

In actual engineering, consumers concern more about the restart ability of induction motor on different sag durations. The maximum-allowed sag duration is defined as the critical clearance time. An analytical algorithm is used in [21] to calculate the critical clearance time during different sag magnitudes. However, corresponding phase-angle jumps are not considered. Fig. 6 shows critical clearance times for 5.5 kW, 55 kW and 135 kW motors under symmetrical voltage sags with considering phase-angle jumps during sag process with the magnitude varying from 10% to 70%.

From Fig. 6, it can be seen that critical clearance time becomes shorter and the ability of riding through voltage sag becomes weaker, when considering phase-angle jump. That is because inrush torque caused by voltage sag affects the stability operation of the induction motor. With phase-angle jump, higher inrush torque is produced, which influences the stability of the motor more seriously and extend recovery time. Taking 135 kW motor at full load as an example, in sag magnitude 70%, the critical clearance time difference between with and without considering phase-angle jump is about 0.13s.

From above analysis, the phase-angle jump has obvious effect on peak current, peak torque, speed loss and critical clearance time. The results between with and without considering phase-angle jump are obviously different. So, the effects of the corresponding phase-angle jump on safe and stable operation of motors cannot be overlooked.

V. EFFECTS OF INITIAL POINT-ON-WAVE

A. EFFECTS OF INITIAL POINT-ON-WAVE ON PEAK CURRENT

Initial point-on-wave −90° ∼90° and 90° ∼270° are symmetrical. Therefore, only −90° ∼90° are considered in this

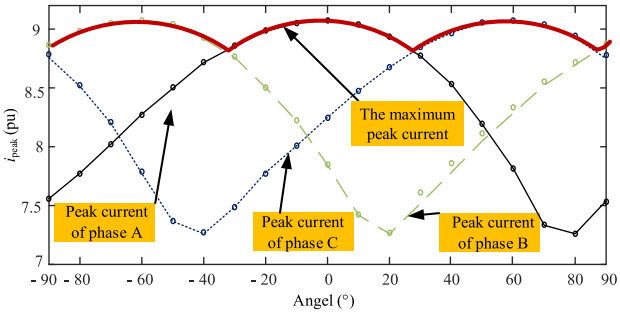

FIGURE 7. Influence of initial point-on-wave 5.5kW motor's current peak.

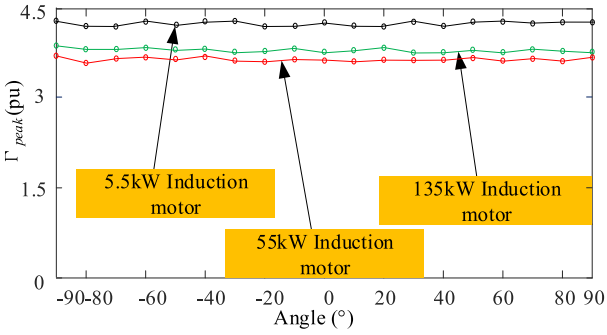

FIGURE 8. Influence of initial point-on-wave on the 5.5kW,55kW and 135kW motor's torque peak.

paper. The 5.5 kW, 55 kW and 135 kW induction motors follow the same rules about the effect of initial point-on-waves on peak current. Taking 5.5kW motor with full load as an example, Fig. 7 shows peak current produced by symmetrical voltage sags with magnitude (30%), duration (0.1s) and phase-angle jump (−43°). From Fig. 8, it can be concluded that

1) With the initial point-on-wave ranging from −90° to 90°, peak current of phase A fluctuates significantly. The value of peak current reach to maximum in 0° and reach to

minimum in 80°.The fluctuation is nearly 15% of the average value.

2) As for the maximum value of three phase peak current, the appear time point of maximum peak current of A, B, C is different. So, the fluctuation of the maximum value of three phase peak current is obviously slight, compared to that of phase A peak current.

To analysis the effects of initial point-on-wave on peak current. The standard deviation is used to describe the fluctuation of peak current:

$$\varepsilon = \sqrt{\frac{1}{n}\sum_{j=1}^{n}\left(i_j - \bar{i}\right)^2} \tag{21}$$

where $\boldsymbol{i}$ represent peak current produced by voltage sags with different initial point-on-waves, $\boldsymbol{i} = [i_1, i_2 \ldots i_n]^{\mathrm{T}}$. The 5.5 kW motor with full load is analysis by using (22) in different sag magnitudes (10%∼90%). The results are shown in Table 2 and it can be seen that the initial point-on-wave nearly has a slight influence on the maximum peak current of three phase ($\varepsilon \approx 0.2$).

TABLE 2. Influence of initial point-on-wave on the 5.5 kW's max value of three phase current peak.

Usag	0.9	0.7	0.5	0.3	0.1
ε	0.1923	0.1842	0.1768	0.1994	0.1927

B. EFFECTS OF INITIAL POINT-ON-WAVE ON PEAK TORQUE, SPEED LOSS AND CRITICAL CLEARANCE TIME

In this paper, taking 5.5 kW, 55 kW and 135 kW motor (full load) with sag magnitude 30% and phase-angle jump −43° as an example, the results are shown in Fig. 8 - Fig. 10 after numerous simulations. It can be found that under different initial point sag processes, the motor's peak torque, minimum speed and critical clearance time are nearly the same. So, it can summarize that the initial point-on-wave only has a slight influence on these three operation indicators, namely peak torque, speed loss and critical clearance time.

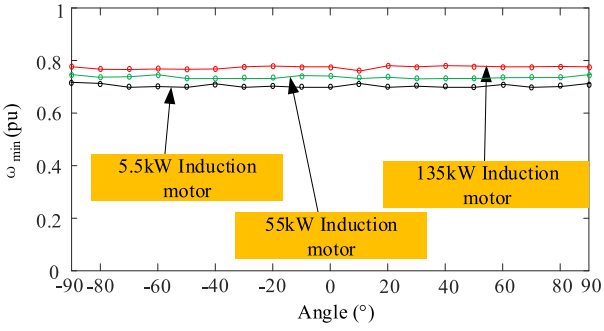

FIGURE 9. Influence of initial point-on-wave on the 5.5kW, 55kW and 135kW motor's speed loss.

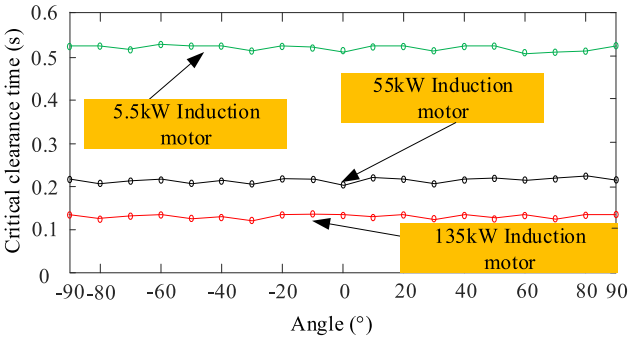

FIGURE 10. Influence of initial point-on-wave on the 5.5kW, 55kW and 135kW motor's critical clearing time.

Referring to the starting process and three phase short circuit of induction motor analysis in [38], [39], under symmetrical voltage sags, the variable of initial point-on-wave can be eliminated during analytical derivation process. Therefore, it can be concluded that the influence of initial point-on-wave under symmetrical voltage sags on these indicators and the wear of induction motor is slight. However, under unsymmetrical voltage sags process, this point-on-wave has an obvious influence on the current and torque peaks and little influence on the speed loss [26].

VI. EXPERIMENTAL VERIFICATION

A. EXPERIMENTAL SCHEME

In this paper, an experimental study of 5.5 kW induction motor is applied for verifying the accuracy. Chroma 18600 programmable power source with 60 kVA rated power is used to generate voltage sag waveform. Power analyser is used to measure the operating performance under steady-state condition. A torque transducer is used to measure the transient torque and speed, and steady-state torque and speed can be read directly from the torque meter. Meanwhile, the transient waveforms, such as stator current, terminal voltage, torque and speed in voltage sag process, can be recorded by the oscilloscope. The test rig is shown in Fig. 11. The experimental schemes are

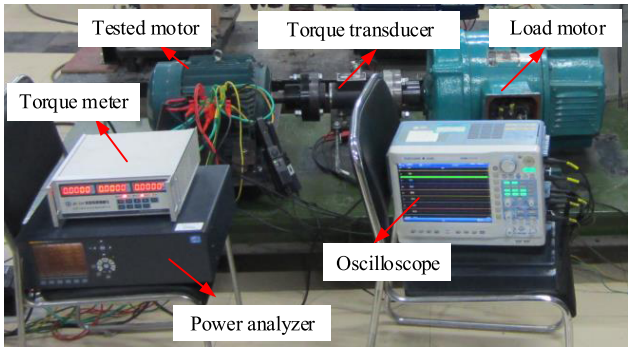

FIGURE 11. Test rig.

1) An experimental test platform for the voltage sag, which includes a programmable three-phase power supply, an oscilloscope, a torque instrument, an induction motor and a DC load motor is provided.

2) By programming the programmable power supply, the different forms of voltage sag can be generated.

B. SIMULATION INTRODUCTION

In this section, the same 5.5 kW induction motor model is used to study the transient performance of induction motors under symmetrical voltage sag process. The detailed specifications of 5.5 kW induction motor are shown in Table 3. And the 2D finite element mesh division is shown in Fig. 12. The finite element model adopts the same excitation terminal voltage waveforms of the real experiment.

TABLE 3. Specification of the 5.5kW induction motor.

Number of poles	4
Number of phases	3
Number of stator slots	36
Number of rotor slots	32
Stator outer diameter	210 mm
Stator bore diameter	136 mm
Active stator stack length	115 mm
Air-gap length	0.4 mm
Rotor Length	117 mm
Rated output power	5.5 kW
Rated current	11.64 A
Rated voltage	380V
Stator winding connection	Delta
Rated speed	1440 r/min

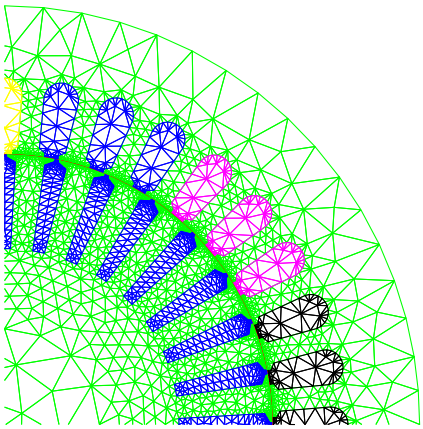

FIGURE 12. 2D Finite element model of the 5.5 kW induction motor.

C. COMPARISON OF EXPERIMENTAL AND SIMULATION RESULTS

The comparison of experimental and simulation results is shown in Fig. 13. It is obvious that the simulation waveform matches well with the measurement ones. Two waveforms have similar tendencies and values. From the Fig. 13, it can be seen that the simulated and test waveforms are not standard sinusoidal waveform. This is because the harmonic waves caused by nonlinear behaviours of magnetic materials and inhomogeneous distribution of magnetic potential and magnetic resistance, which can be accurately calculated by the proposed method. The more details (current peak, torque peak and minimum speed) of the 5.5kW motor under voltage sag process are shown in Table 4.

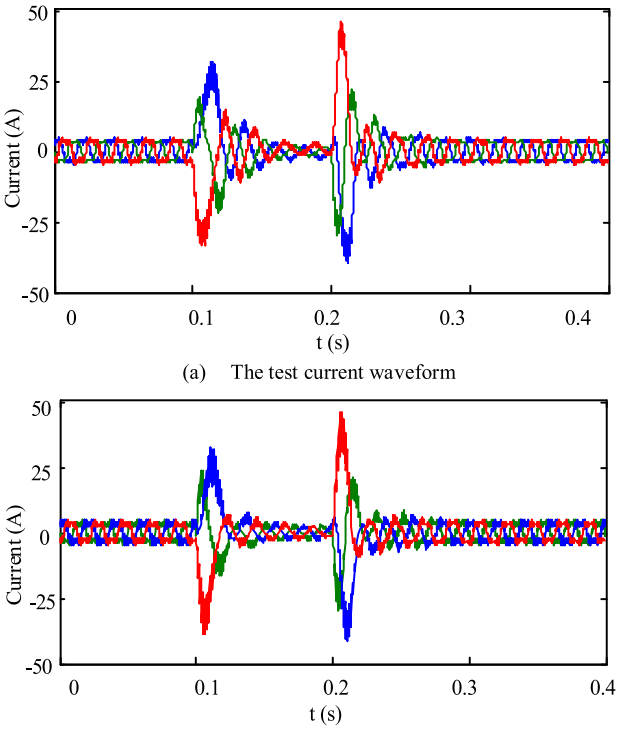

(a) The test current waveform

(b) The current waveform calculated by the proposed method

FIGURE 13. Comparison between the measured and calculated stator currents of the 5.5kW induction motor with initial point-on-wave, no phase-angle jump, no-load condition and 50% magnitude.

TABLE 4. Comparison of simulation and experiment voltage Sag 50% magnitude, no phase angle jump and no load.

Initial point-on-wave	Peak Current (A)		Peak Torque (Nm)		Minimum Speed (r/min)	
	Simulation	Test	Simulation	Test	Simulation	Test
0°	46.57	46.9	91.19	91.8	1404	1410
90°	46.1	45.8	90.8	91.5	1400	1406

VII. CONCLUSION

This paper adopts new 2-D multi-slice time-stepping FEM to study the influence of phase-angle factors on the performance of induction motor during the voltage sag process. As the symmetrical voltage sag is the most severe sag event, this paper only considers the symmetrical voltage sag process. The simulation results not only can calculate the fundamental wave, but also take the harmonic components into account. In addition, taking three types motors: a 5.5 kW (small), a 55 kW (medium) and a 135 kW (large) induction motors as examples, this paper has a detailed exposition on the

effects of phase-angle jump and initial point-on-wave on the value of peak current and peak torque, the minimum motor speed and critical clearance time of the induction motor. The results show that the 1) Not considering the corresponding phase-angle jump will cause significant errors on the value of peak current, peak torque, speed loss and critical clearing time. For example, at some sag magnitudes, such as 50% sag magnitude, the torque peak and current peak is nearly 1.5∼2 times as much as that without considering phase angle jump. Therefore, in the future study, the phase-angle jump corresponding to each voltage sag process is also an important influence factor. 2) The initial point-on-wave nearly has a slight influence on peak current ($\varepsilon \approx 0.2$). The main reason is that three phase stator windings are symmetric in space. Under the symmetrical sag process, the three-phase peak current appears at different times intervals, which are complementary to each other. The initial point-on-wave nearly has no influence on peak torque, speed loss and critical clearance time. This is because the initial point-on-wave variable can be eliminated during analytical derivation process. In the future, we will further how to set up the protection devices to protect the motor from the influence of phase angle jump.

REFERENCES

[1] J. Wang, Z. Xu, and Y. Che, "Power quality disturbance classification based on compressed sensing and deep convolution neural networks," *IEEE Access*, vol. 7, pp. 78336–78346, 2019.

[2] B. Zhou and R. Gong, "Study on pricing method of power quality differentiated market service in distribution grid," *IEEE Access*, vol. 7, pp. 147021–147028, 2019.

[3] T. Liu, D. Zhang, and T. Wu, "Standardised modelling and optimisation of a system of interconnected energy hubs considering multiple energies–electricity, gas, heating, and cooling," *Energy Convers. Manage.*, vol. 205, Feb. 2020, Art. no. 112410.

[4] *IEEE Recommended Practice for Voltage Sag and Short Interruption Ride-Through Testing for End-Use Electrical Equipment Rated Less Than 1000 V*, IEEE Standard 1668-2017, Revision of IEEE Standard 1668-2014, Nov. 2017, pp. 1–85.

[5] Y. He, Y. Xu, and J. Chen, "Improved space vector modulation of quasi Z-Source inverter to suppress DC-link voltage sag," *IEEE Access*, vol. 7, pp. 66689–66702, 2019.

[6] T. Liu, D. Zhang, H. Dai, and T. Wu, "Intelligent modeling and optimization for smart energy hub," *IEEE Trans. Ind. Electron.*, vol. 66, no. 12, pp. 9898–9908, Dec. 2019.

[7] Y. Wang, A. Bagheri, M. H. J. Bollen, and X.-Y. Xiao, "Single-event characteristics for voltage dips in three-phase systems," *IEEE Trans. Power Del.*, vol. 32, no. 2, pp. 832–840, Apr. 2017.

[8] Y. Han, Y. Feng, P. Yang, L. Xu, Y. Xu, and F. Blaabjerg, "Cause, classification of voltage sag, and voltage sag emulators and applications: A comprehensive overview," *IEEE Access*, vol. 8, pp. 1922–1934, 2020.

[9] J. R. Camarillo-Peñaranda and G. Ramos, "Fault classification and voltage sag parameter computation using voltage ellipses," *IEEE Trans. Ind. Appl.*, vol. 55, no. 1, pp. 92–97, Jan. 2019.

[10] Y. Xu, W. Lu, K. Wang, C. Li, and W. Aslam, "Sensitivity of low-voltage variable-frequency devices to voltage sags," *IEEE Access*, vol. 7, pp. 2068–2079, 2019.

[11] S. Shakeri, S. Esmaeili, and M. H. R. Koochi, "Voltage sag assessment considering low voltage ride-through requirement for wind turbines based on SARFI index," in *Proc. 27th Iranian Conf. Electr. Eng. (ICEE)*, Yazd, Iran, Apr. 2019, pp. 470–474.

[12] P. Li, L. Xie, J. Han, S. Pang, and P. Li, "A new voltage compensation philosophy for dynamic voltage restorer to mitigate voltage sags using three-phase voltage ellipse parameters," *IEEE Trans. Power Electron.*, vol. 33, no. 2, pp. 1154–1166, Feb. 2018.

[13] A. Parreño Torres, P. Roncero-Sánchez, J. Vázquez, F. J. López-Alcolea, and E. J. Molina-Martínez, "A discrete-time control method for fast transient voltage-sag compensation in DVR," *IEEE Access*, vol. 7, pp. 170564–170577, 2019.

[14] H. Liao, S. Abdelrahman, Y. Guo, and J. V. Milanović, "Identification of weak areas of power network based on exposure to voltage sags—Part I: Development of sag severity index for single-event characterization," *IEEE Trans. Power Del.*, vol. 30, no. 6, pp. 2392–2400, Dec. 2015.

[15] H. Liao, S. Abdelrahman, Y. Guo, and J. V. Milanović, "Identification of weak areas of network based on exposure to voltage sags—Part II: Assessment of network performance using sag severity index," *IEEE Trans. Power Del.*, vol. 30, no. 6, pp. 2401–2409, Dec. 2015.

[16] P. Thakur, A. K. Singh, and R. C. Bansal, "Novel way for classification and type detection of voltage sag," *IET Gener., Transmiss. Distrib.*, vol. 7, no. 4, pp. 398–404, Apr. 2013.

[17] S. Hasan, K. M. Muttaqi, and D. Sutanto, "Automated segmentation of the voltage sag signal using Hilbert Huang transform to calculate and characterize the phase angle jump," in *Proc. IEEE Ind. Appl. Soc. Annu. Meeting*, Baltimore, MD, USA, Sep. 2019, pp. 1–6.

[18] A. P. Torres, P. Roncero-Sànchez, and V. F. Batlle, "A two degrees of freedom resonant control scheme for voltage-sag compensation in dynamic voltage restorers," *IEEE Trans. Power Electron.*, vol. 33, no. 6, pp. 4852–4867, Jun. 2018.

[19] A. M. Rauf and V. Khadkikar, "An enhanced voltage sag compensation scheme for dynamic voltage restorer," *IEEE Trans. Ind. Electron.*, vol. 62, no. 5, pp. 2683–2692, May 2015.

[20] D. Zhang and T. Liu, "Effects of voltage sag on the performance of induction motor based on a new transient sequence component method," *China Electrotech. Soc. Trans. Electr. Mach. Syst.*, vol. 3, no. 3, pp. 316–324, Sep. 2019.

[21] Z. Wang, X. Wang, and C. Y. Chung, "An analytical method for calculating critical voltage sag clearance time of induction motors," *IEEE Trans. Power Del.*, vol. 27, no. 4, pp. 2412–2414, Oct. 2012.

[22] L. Tianhao and L. Gengyin, "Stator current transient performance of induction motor under different voltage sag conditions," in *Proc. Int. Conf. Renew. Power Gener. (RPG)*, Beijing, China, 2015, pp. 1–5.

[23] A. Rolán, F. Córcoles, and J. Pedra, "Doubly fed induction generator subject to symmetrical voltage sags," *IEEE Trans. Energy Convers.*, vol. 26, no. 4, pp. 1219–1229, Dec. 2011.

[24] F. Corcoles and J. Pedra, "Algorithm for the study of voltage sags on induction machines," *IEEE Trans. Energy Convers.*, vol. 14, no. 4, pp. 959–968, Dec. 1999.

[25] M. Ojaghi, J. Faiz, H. Shahrouzi, and S. Alimohammadi, "Induction motors performance study under various voltage sags using simulation," *J. Int. Conf. Electr. Mach. Syst.*, vol. 1, no. 3, pp. 295–302, Sep. 2012.

[26] L. Guasch, F. Corcoles, and J. Pedra, "Effects of symmetrical and unsymmetrical voltage sags on induction machines," *IEEE Trans. Power Del.*, vol. 19, no. 2, pp. 774–782, Apr. 2004.

[27] J. Pedra, F. Corcoles, and L. Sainz, "Effects of unsymmetrical voltage sags on squirrel-cage induction motors," *IET Gener., Transmiss. Distrib.*, vol. 1, no. 5, pp. 769–775, 2007.

[28] L. Guasch, F. Corcoles, and J. Pedra, "Effects of unsymmetrical voltage sag types E, F and G on induction motors," in *Proc. 9th Int. Conf. Harmon. Qual. Power*, vol. 3, Aug. 2019, pp. 796–803.

[29] J. Pedra, L. Sainz, and F. Córcoles, "Effects of symmetrical voltage sags on squirrel-cage induction motors," *Electr. Power Syst. Res.*, vol. 77, no. 12, pp. 1672–1680, Oct. 2007.

[30] J. V. Milanovic, M. T. Aung, and S. C. Vegunta, "The influence of induction motors on voltage sag propagation—Part I: Accounting for the change in sag characteristics," *IEEE Trans. Power Del.*, vol. 23, no. 2, pp. 1063–1071, Apr. 2008.

[31] J. V. Milanovic, S. C. Vegunta, and M. T. Aung, "The influence of induction motors on voltage sag propagation—Part II: Accounting for the change in sag performance at LV buses," *IEEE Trans. Power Del.*, vol. 23, no. 2, pp. 1072–1078, Apr. 2008.

[32] J. C. Gomez, M. M. Morcos, C. A. Reineri, and G. N. Campetelli, "Behavior of induction motor due to voltage sags and short interruptions," *IEEE Trans. Power Del.*, vol. 17, no. 2, pp. 434–440, Apr. 2002.

[33] D. Zhang, T. Liu, C. He, and T. Wu, "A new 2-D multi-slice time-stepping finite element method and its application in analyzing the transient characteristics of induction motors under symmetrical sag conditions," *IEEE Access*, vol. 6, pp. 47036–47046, 2018.

[34] D. Zhang, T. Liu, H. Zhao, and T. Wu, "An analytical iron loss calculation model of inverter-fed induction motors considering supply and slot harmonics," *IEEE Trans. Ind. Electron.*, vol. 66, no. 12, pp. 9194–9204, Dec. 2019.

[35] D. Zhang, H. Dai, H. Zhao, and T. Wu, "A fast identification method for rotor flux density harmonics and resulting rotor iron losses of inverter-fed induction motors," *IEEE Trans. Ind. Electron.*, vol. 65, no. 7, pp. 5384–5394, Jul. 2018.
[36] Y. Xu, *Voltage Sags and Short Interruptions in Power Grid*. Beijing, China: China Electric Power Press, 2018, pp. 69–75.
[37] Y. Huangfu, S. Wang, J. Qiu, H. Zhang, G. Wang, and J. Zhu, "Transient performance analysis of induction motor using field-circuit coupled finite-element method," *IEEE Trans. Magn.*, vol. 50, no. 2, pp. 873–876, Feb. 2014.
[38] Y. Tang, *Dynamic Analysis of AC Motor*. Beijing, China: Mechanical Engineering Press, 2004.
[39] A. M. Wahl and L. A. Kilgore, "Transient starting torques in induction motors," *Trans. Amer. Inst. Electr. Eng.*, vol. 59, no. 11, pp. 603–607, Nov. 1940.

TIANHAO LIU (Member, IEEE) was born in Shanxi, China, in 1990. He received the B.Eng. and M.S. degrees in electrical engineering and automation from the College of Electrical Engineering, North China Electric Power University, in 2013 and 2016, respectively. He is currently pursuing the Ph.D. degree in electrical engineering with Hong Kong University.

He worked as an Assistant Researcher with the Southern Power Grid Research Institute, in 2017. His research interests include motor system optimal operation, the modeling and optimization of multiple energy system, and energy market.

MEIHUI JIANG was born in Guangxi, China, in 1994. She received the B.B.A. degree from the Qingdao University of Technology, Shandong, China, in 2016, and the M.E. degree in logistics engineering from Guangxi University, in 2019.

She currently works with the Nanning Fright Center, China Railway Nanning Group Company, Ltd. Her research interests include the artificial intelligence and its application on the design of enterprise logistic structure and supplier outspreading model, electrical machines, and its driving system design.

DONGDONG ZHANG (Member, IEEE) was born in Jining, China, in 1990. He received the B.Eng. degree in electrical engineering and automation from the College of Electrical Engineering, Qilu University of Technology, Shandong, China, in 2013, the M.S. degree in electric power system and automation from North China Electric Power University, in 2016, and the Ph.D. degree in electrical engineering from Xi'an Jiaotong University, in 2019.

He is currently an Assistant Professor with Guangxi University. His research interests include the modeling and optimization of multiple energy systems, energy market, and electrical machines and its driving system design.

HAISEN ZHAO (Senior Member, IEEE) was born in Hebei, China, in 1982. He received the B.S.E.E degree from the Agriculture University of Hebei, in 2004, and the Ph.D. degree in electronic engineering from North China Electric Power University, Beijing, China, in 2011.

He is currently an Associate Professor with North China Electric Power University. His research interests include electrical machines design, operation performance and energy consumption analysis on electric machines, and motor system energy saving.

FENG SHUANG received the B.S. degree from the Special Class of Gifted Young, University of Science and Technology of China (USTC), in 1995, and the Ph.D. degree from the Department of Chemical Physics, USTC, in 2000.

He was a Research Associate with Princeton University, from 2001 to 2003, and was a Research Staff Member at Princeton University, from 2004 to 2009. In 2009, he joined the Institute of Intelligent Machines (IIM), China, as a Full Professor, and then was selected as a member of the One Hundred Talented People of Chinese Academy of Sciences. He is currently a Professor with Guangxi University. He has published more than 50 articles and applied more than ten national invention patents. His research interests include system control and information acquisition, including multidimensional force sensors, quantum system control, quantum measurements, and so on.